Rare Metal Materials and Engineering
Volume 55, Issue 4, April 2026
Available online at www.rmme.ac.cn

Science Press

Cite this article as: Cao Likun, Yang Fang, Hao Qingbin, et al. Research Progress of Ta-Nb-Hf-Zr-Ti High Entropy Alloy Superconductors[J]. Rare Metal Materials and Engineering, 2026, 55(04): 926-940. DOI: https://doi.org/10.12442/j.issn.1002-185X.20250130.

REVIEW

Research Progress of Ta-Nb-Hf-Zr-Ti High Entropy Alloy Superconductors

Cao Likun[1,2], Yang Fang[1], Hao Qingbin[2], Zhang Shengnan[2], Yan Guo[1,3], Zhang Pingxiang[1,2]

[1] Institute of Superconducting Materials and Applied Technology, Northwestern Polytechnical University, Xi'an 710072, China; [2] Superconducting Materials Research Center, Northwest Institute for Nonferrous Metal Research, Xi'an 710016, China; [3] Xi'an Juneng Medical Engineering Technologies Co., Ltd, Xi'an 710028, China

Abstract: High-entropy alloys, a novel class of materials characterized by the statistical distribution of multiple principal elements on simple crystalline lattices, have emerged as a research hotspot in materials science and condensed matter physics due to their exceptional mechanical properties and unique high-entropy characteristic. Since the discovery of the first high-entropy superconductor in 2014, exploring their superconducting performance and advantages has progressively become a frontier in scientific research. The Ta-Nb-Hf-Zr-Ti system, in particular, exhibits remarkable mechanical robustness, outstanding radiation tolerance, and superconducting performance comparable to the binary NbTi alloy, positioning it as a promising candidate for advanced applications, such as high-field superconducting magnets, superconducting electric motors, and next-generation nuclear fusion reactors. This review systematically summarized global research progress on Ta-Nb-Hf-Zr-Ti-based superconductors, aiming to provide a comprehensive reference for advancing this burgeoning field.

Key words: high-entropy alloys; Ta-Nb-Hf-Zr-Ti; superconductor

1 Introduction

Breaking through the restrictions of traditional single-principal-element alloy systems, Yeh[1] and Cantor[2] et al first proposed the innovative concept of high-entropy alloys (HEAs) in 2004. The design philosophy of HEAs aims to enhance configurational entropy through the incorporation of multiple principal elements. The lattice will become stable when the entropy increase sufficiently counteracts the enthalpy of compound formation[3]. Excessive lattice distortion may induce phase transitions from solid solutions to amorphous alloys or crystal/glass composites[4]. HEAs generally exhibit superior properties including high hardness, exceptional strength, outstanding corrosion/radiation resistance, and remarkable low-temperature mechanical performance[5], demonstrating broad application prospects. Since the discovery of superconductivity in mercury (1911), superconducting materials have evolved into cuprate- and iron-based systems. Current superconducting materials face several critical challenges.

1) Low transition temperatures: most of HEAs operate below liquid helium temperatures (4.2 K), with some requiring ultrahigh pressures to exhibit superconductivity, severely restricting practical applications.

2) Incomplete mechanistic understanding: the superconducting mechanisms, particularly for high-temperature superconductors (superconducting transition temperature, T_c>77 K), remain elusive, hindering theoretically guided material design and optimization.

3) Complex synthesis routes: many HEAs require intricate preparation processes and incur high costs, restricting scalable production.

4) Mechanical property constraints: inherent mechanical restrictions narrow application scopes and shorten service

Received date: April 12, 2025
Foundation item: Northwest Institute of Nonferrous Metal Research Funding (YK2324); Key Research and Development Program of Shaanxi (2024GX-YBXM-403); National Natural Science Foundation of China (52277029)
Corresponding author: Hao Qingbin, Ph. D., Professor, Superconducting Materials Research Center, Northwest Institute for Nonferrous Metal Research, Xi'an 710016, P. R. China, E-mail: haoqb@c-nin.com

lifetimes.

5) Technological immaturity: despite advancements in specific areas, overall technological maturity remains low, necessitating further innovation.

The first HEAs were discovered by Kozelj et al[6] in 2014, and this new class of materials led to explosive research into high-entropy superconductors[7–8]. HEAs retain the excellent mechanical properties, such as high strength and high toughness. At the same time, HEAs exhibit good superconducting stability under high pressure and high magnetic fields, which makes them more potential under extreme conditions. In addition, the reported components of HEAs are safe and non-toxic, and the preparation method is relatively simple. From the perspective of Matthias' rule, HEAs composed of transition metals can be regarded as intermediate materials between transition metal crystal superconductors and amorphous superconductors[9]. The study of HEAs is helpful to further understand the influence of high-entropy effect on superconductivity, enrich the theory of superconductivity, further understand the nature and mechanism of superconductivity, and promote the development of superconductors, HEAs, and condensed matter physics. In addition, HEAs component regulation has infinite possibilities, and the design and customization of superconductors with specific properties have greater freedom, which provides new ideas and methods for designing new superconductors. In this review, the research achievements of Ta-Nb-Hf-Zr-Ti system since the discovery of the first high-entropy superconductor were introduced.

The innovation of HEAs marks the first deep fusion of two breakthrough concepts in materials science: high-entropy effect and superconducting quantum coherence. This multi-principal disordered system not only challenges the rigid requirement of traditional superconductors for structural order degree, but also reveals the delicate balance between the lattice stability dominated by configurational entropy and the electron-phonon coupling (EPC) strength. Through the exploration of Ta-Nb-Hf-Zr-Ti system, researchers have gradually verified the unique role of high entropy in regulating the order parameters of superconductivity, providing a new experimental platform for understanding the mechanism of high-temperature superconductivity.

2 Definition and Characteristic of HEAs

Since Yeh et al[1] first proposed the concept of HEA, its definition has gradually expanded to the dual perspectives of composition and entropy. (1) Compositional definition: systems contain at least five (up to 13) principal elements, each with atomic percentage ranging from 5% to 35%[10]. (2) Entropy-based classification: an extended framework proposed by Sun et al[7] generalizes HEAs into three categories:

1) Low-entropy alloys: n=3, $\Delta S_{mix}<0.69R$

2) Medium-entropy alloys: n=4, $0.69R\leqslant\Delta S_{mix}\leqslant1.59R$

3) HEAs: $n\geqslant5$, $\Delta S_{mix}>1.59R$

where R denotes the gas constant (8.314 $J\cdot mol^{-1}\cdot K^{-1}$) [11], n denotes the number of types of elements, and ΔS_{mix} denotes the mixing entropy. Although boundary discrepancies exist (e. g., Yeh[12] suggested $\Delta S_{mix}>1.5R$), this framework establishes unified criteria for phase stability prediction. Face-centered cubic (fcc)-structured HEAs predominantly originate from CoCrFeMnNi-based systems and their derivatives, whereas body-centered cubic (bcc) -structured HEAs mainly derive from quaternary, pentanary, hexanary, and septenary components[13].

The cocktail effect (multi-component synergistic strengthening) and lattice distortion effect (local strain fields induced by atomic size mismatch) constitute the core characteristics distinguishing HEAs from conventional alloys. In superconducting systems, the cocktail effect broadens the density of states (DOS) near the Fermi surface through multi-element orbital hybridization. The lattice distortion effect enhances EPC strength by amplifying phonon anharmonicity. This ordered disorder characteristic enables HEAs to maintain crystalline long-range order while exhibiting strong coupling features analogous to amorphous systems.

Reported Ta-Nb-Hf-Zr-Ti HEAs typically have a bcc structure, with a space group of $Im\bar{3}m$ (No. 229) and a lattice constant of $\alpha\approx0.34$ nm[14]. This structure significantly impacts their superconductivity. The bcc structure, resulting from multiple elements randomly occupying lattice sites, causes severe lattice distortion. Moreover, the low atomic packing factor of 68% enhances superconductivity stability under high pressure. The sparse atomic arrangement boosts the electronic DOS and strengthens EPC, favoring superconductivity. The bcc Ta-Nb-Hf-Zr-Ti superconductors usually exhibit a high upper critical field (H_{c2}) and a low lower critical field (H_{c1}). For instance, $Ta_{1/6}Nb_{2/6}Hf_{1/6}Zr_{1/6}Ti_{1/6}$ has an $H_{c2}(0)$ of 12.05 T and an $H_{c1}(0)$ of 23 mT[15]. Electronic structure calculations show that despite significant chemical disorder, the electronic bands remain sharp with minimal bandwidth, indicating stability and consistency in the electronic structure of bcc HEAs. Some Ta-Nb-Hf-Zr-Ti HEAs feature non-centrosymmetric structures, such as the α-Mn type, which generally exhibit a high H_{c2} and strong EPC strength[16].

3 Fabrication Methods of Ta-Nb-Hf-Zr-Ti HEAs

3.1 Conventional fabrication techniques

3.1.1 Arc melting

Arc melting can achieve instantaneous melting of difficult metals through the non-transfer arc generated between tungsten electrode and metal raw materials (current density of 10^2-10^3 A/cm^2; arc temperature of 3000 – 5000 K), and its cooling rate can reach 10^3–10^4 K/s. Through precise control of melting parameters, the melting process can achieve instant melting. It can achieve uniform mixing of alloys, and the method is widely used in the preparation of various metal materials. In the early research of Ta-Nb-Hf-Zr-Ti HEAs, arc melting is the most commonly used preparation method. This method has the advantages of high melting temperature, good chemical uniformity, and low cost. However, its disadvantage

is that it is difficult to accurately control the microstructure of the alloy, such as grain size and phase distribution. Generally, in order to further optimize the properties of the alloy, it is necessary to combine subsequent heat treatment or other processing methods. Because the elements constituting HEAs often have high melting points, these refractory metals present a challenge to melting and diffusion while providing unexpected properties. Therefore, using arc melting to melt the proportionally prepared metal is the most common way to prepare HEAs. Typically, this process requires multiple melting, during which the mixture is repeatedly turned over to ensure a uniform mixture[7]. In addition, the cooling rate also needs to be controlled during solidification to match its high entropy characteristics.

3.1.2 High-energy ball milling

High-energy ball milling, or mechanochemistry method, mechanically mixes metallic powders to form uniform precursor powders, circumventing elemental segregation and phase separation problems inherent in melting processes. This technique is particularly suited for nanostructured materials. Drawbacks include prolonged processing times and potential impurity incorporation.

3.1.3 Spark plasma sintering (SPS)

SPS is an advanced rapid sintering technique, which is widely used to prepare various high-performance materials, including HEAs, ceramics, and composites. It realizes the rapid densification of materials through the plasma effect and pressure produced by pulsed current. This method has the advantages of short preparation time, controllable grain size, and uniform composition. HEAs prepared by SPS technique show excellent superconductivity and mechanical properties, but there are some restrictions in equipment cost and sample size.

3.1.4 Powder-in-tube (PIT)

Superconducting wire can conduct large current without energy loss, so it has a wide application prospect in the fields of industry, medical treatment, and scientific research. Traditional superconductors, such as NbTi and Nb_3Sn, have restricted their applications due to the rapid decrease in critical current density or greater brittleness under magnetic field. Ta-Nb-Hf-Zr-Ti HEAs have high critical current density J_c, which have potential application value in the field of superconducting wires. PIT is a common method for preparing superconducting wires. It has the advantages of simple operation, low cost, and large-scale production. It plays an important role in the preparation of superconducting tapes. With the progress of technology, it shows great potential in the preparation of high-performance superconductors. Kovalev et al[17] pioneered Ta-Nb-Hf-Zr-Ti HEA wire using PIT, highlighting its scalability and industrial potential including the following three steps. (1) Powder synthesis: Ta-Nb-Hf-Zr-Ti HEAs powder was produced via high-energy planetary ball milling (400 r/min for 12 h); (2) tube filling and drawing: powder-loaded iron tubes were drawn into 1 mm-diameter wires; (3) sintering: wire segments (length of 30 mm) were vacuum-sintered in quartz tubes (600–1000 °C for 0.5–12 h).

3.2 Advanced fabrication strategies

3.2.1 Magnetron sputtering

Zhang et al[5] reported the research results of $(TaNb)_{1-x}$-$(ZrHfTi)_x$ thin films prepared by direct current sputtering for the first time. Prior to this, the preparation of HEAs mainly depended on the arc melting technique in inert gas atmosphere, which greatly restricted the manufacturing and application prospects of superconducting electronic devices. Magnetron sputtering[4–5,18–19] is a material preparation method by bombarding the target with high-energy ion beam to make the target atoms sputter and deposit on the substrate to form a thin film. The advantage of this method is that it can form a uniform HEA film, and can accurately control the microstructure of the film according to the given growth parameters, so as to realize the effective regulation of the film performance, which is more stable than the deposition of bulk samples[20].

3.2.2 Pulsed laser deposition (PLD)

PLD is a physical vapor deposition technique. Its basic principle is to irradiate the target with high energy density laser pulses, so the material on the surface of the target can evaporate or sublimate instantaneously, forming high-temperature and high-pressure plasma. These evaporated materials are driven by laser pulses to move towards the substrate surface at a high speed and to form thin films on the substrate. Due to the high energy and short duration of the laser pulse (usually on the nanosecond scale), the material on the surface of the target can evaporate rapidly, thus reducing the decomposition and oxidation of the material in the evaporation process, and ensuring the purity and quality of the film. In addition, PLD has the advantages of fast deposition rate and strong controllability, which can produce high-purity films with excellent properties. This method is suitable for the preparation of thin films of metals, ceramics, semiconductors, and other materials. It is commonly used to prepare superconducting thin films in the superconducting field, such as high-temperature superconductors and iron-based superconductors. PLD method can ensure that the chemical composition of the film is basically the same as that of the target, effectively avoiding the preferential evaporation effect of the composition and the spatial constraint effect of the plasma emission along the axis of the target, so it is very suitable for preparing multi-component compound films containing volatile elements.

To sum up, compared with the traditional melting method, the breakthroughs in film preparation techniques, such as magnetron sputtering and PLD, have achieved atomic level composition control, marking the strategic transformation of HEAs from bulk materials to functional devices. Traditional preparation methods show advantages in bulk preparation. The core contradiction of technical iteration is the balance between large-scale production and performance restriction breakthrough.

3.2.3 Additive manufacturing (AM)

AM[21–25], also known as 3D printing, fundamentally differs from traditional manufacturing methods that rely on cutting or removing material. AM builds 3D objects by gradually stacking or adding material layer by layer. In metal 3D printing, a laser or electron beam is typically used as a heat source to melt metal powders, and the product is prepared layer by layer. Common metal 3D printing techniques include selective laser melting, direct metal deposition, and electron beam melting. Laser engineered net shaping (LENS) [26] involves a computer-controlled laser beam to scan a metal powder bed, precisely ejecting the powder, which is then melted, deposited by the laser, and solidified. After each layer is printed, the worktable lowers by a layer thickness, and new powder is spread over the solidified layer. This process is repeated until the part is fully formed. In the field of superconductors, direct writing printing has become a viable method for preparing yttrium barium copper oxide superconductors. However, there have been few reports of AM technique to prepare HEAs. Our team is currently conducting experiments to prepare HEAs using LENS and has achieved preliminary results.

4 Factors Influencing Superconducting Properties of Ta-Nb-Hf-Zr-Ti Alloys

As summarized in Table 1, superconducting parameters (e. g., T_c=2 – 9 K) exhibit method-dependent variations even for identical composition[9]. Valence electron concentration (VEC) calculations use elemental VEC values obtained from Ref.[27].

4.1 Elemental doping

Elemental doping studies have revealed the synergistic mechanisms between functional elements and structural-support elements in HEAs. Le et al[30] investigated the superconducting properties of $Ta_{1/6}Nb_{2/6}Hf_{1/6}Zr_{1/6}Ti_{1/6}$ HEA films doped with 0.5% C using PLD. Carbon atoms do not substitute other elements but instead stabilize the lattice as interstitial atoms, increasing T_c from 7.25 K (undoped) to 7.50 K (0.5% C-doped). At zero-temperature limit, the upper critical fields $\mu_0 H_{c2}(0)$ for the undoped and C-doped HEAs are 12.73 and 13.45 T with coherence lengths $\xi(0)$ of 5.08 and 4.95 nm, respectively. Superconducting vortices were observed in the C-doped films but absent in pristine samples. Magnetic penetration depth (λ) measurements at 4.2 K show λ =360 nm for the C-doped film, which is significantly shorter than 560 nm for the undoped film, indicating enhanced magnetic shielding capability.

Kim et al[31] compared the samples prepared by arc melting[15] (Section 3.1.1), ball milling, and SPS process, and found that the J_c of the ball milled sample was significantly increased. Under the conditions of 2 K and 0.01 T, J_c reaches approximately 30 500 A/cm^2, representing a 286% enhancement over arc-melted samples. Under the conditions of 4 K and 0.01 T, J_c increases to approximately 73 200 A/cm^2 (687% improvement). Calculations confirm that SPS-processed

Table 1 Properties of Ta-Nb-Hf-Zr-Ti superconductors

HEA	T_c/K	Upper critical field, $\mu_0 H_{c2}(0)$/T	Lattice parameter, a/nm	VEC	Ref.
$Ta_{34}Nb_{33}Hf_8Zr_{14}Ti_{11}$	7.30	8.20	0.3360	4.67	[6]
	7.30	8.20	0.3360	4.67	[28]
	7.50	12.20	0.3349	4.67	[29]
$Ta_{1/6}Nb_{2/6}Hf_{1/6}Zr_{1/6}Ti_{1/6}$	7.83	10.50	0.3370	4.50	[30–31]
	7.25	12.73	0.3377	4.50	[31]
	7.76	10.28	0.3380	4.50	[32]
	7.28	12.70	0.3358	4.50	[33]
	7.85	12.05	0.3380	4.50	[15,34]
NbTaTiZrHf	7.12 (as-cast) 6.69 (homogenized)	1.85 (5 T)	0.3405 (homogenized)	4.40	[35]
$(TaNb)_{4.78}(ZrHfTi)_{0.22}$	5.6	5.60	0.3360	4.78	[4]
$(TaNb)_{4.60}(ZrHfTi)_{0.40}$	6.7	7.50	0.3374	4.60	
$(TaNb)_{4.31}(ZrHfTi)_{0.69}$	5	8.30	0.3452	4.31	
$(TaNb)_{0.57}(ZrHfTi)_{0.43}$	6.9	8.80	0.3370	4.57	[5]
$(TaNb)_{0.35}(ZrHfTi)_{0.65}$	5.7	11.05	0.3410	4.35	
$(TaNb)_{0.67}(HfZrTi)_{0.33}$	7.7 (at 101.3 kPa) 9 (190.6 GPa)	8 (at 101.3 kPa) 2 (179.2 GPa)	0.3360	4.67	[36]
$Ti_{0.5}(ZrNbHfTa)_{0.5}$	6.0	13.50	0.3365	4.25	[37]
$(TaNb)_{0.31}(TiUHf)_{0.69}$	3.2	6.40	0.3410	4.31	[38]
$Ta_{1/6}Nb_{2/6}Hf_{1/6}Zr_{1/6}Ti_{1/6}$+0.5% C	7.50	13.45	0.3379	-	[31]
$(TaNb)_{0.67}(HfZrTi)_{0.33}Al_{0.15}$	6.7	-	-	4.45	[39]
$TaNb_4HfZr_4Ti_4$	7.6	-	0.3390	4.36	-

samples exhibit significantly higher flux pinning forces, consistent with surface pinning models. The performance enhancement arises not only from microstructural defects and impurity particles formed during SPS but also from Fe-based magnetic phases introduced by stainless steel milling containers, as verified by X-ray diffractometer (XRD).

Von Rohr et al[39] synthesized (HEA)Al_x to study the electron-count dependence of superconducting properties in $(TaNb)_{0.67}(HfZrTi)_{0.33}$. Results showed that increasing Al content reduces the lattice parameter from approximately 0.334 nm (x=0) to 0.329 nm (x=0.4). Sharper diffraction peaks and slightly increased residual resistivity ratio indicate enhanced crystallinity, while T_c decreases with Al doping. VEC-dependent T_c behavior in (HEA)Al_x (x<0.4) falls between crystalline and amorphous superconductors. Compared to $(TaNb)_{1-x}(ZrHfTi)_x$, its T_c dependence on VEC more closely resembles crystalline systems, despite amorphous-like behavior across the solid solution.

Al doping promotes Nb-rich phase formation. According to Matthias' empirical rules, selecting appropriate components with an optimal electron-to-atom ratio (e/a) maximizes T_c. However, in ternary NbTiAl alloys, T_c only marginally exceeds that of binary NbTi, suggesting restricted applicability of Matthias' rules to multi-component alloys. Hidayati et al[40] emphasized the influence of fabrication methods on HEAs performance. Wu et al[35] studied superconducting behavior in equimolar NbTaTiZr-based HEAs, preparing NbTaTiZr, NbTaTiZrHf, NbTaTiZrHfV, and NbTaTiZrHfVMo samples labeled as C-series (as-cast) and H-series (homogenized). Some designations are given. They are equal-molar C4 and H4 for NbTaTiZr, C5 and H5 for NbTaTiZrHf, C6 and H6 for NbTaTiZrHfV, and C7 and H7 for NbTaTiZrHfVMo. Fig.1 and Fig.2 show that adding Hf and V to C4 reduces T_c, with homogenized samples exhibiting lower T_c than that of as-cast counterparts. C7 and H7 show no superconducting transitions between 4.2 and 300 K. Microstructural analysis (Fig.3) reveals that dendritic phases in C4–C6 are Nb-Ta-rich phases, and T_c strongly correlates with total Nb+Ta content. Homogenization reduces Nb+Ta concentration in the matrix phase, lowering T_c below as-cast values. The superconducting properties of HEAs depend not only on Nb+Ta distribution in superconducting phases, but also on lattice distortions and associated Debye temperature (θ_D) changes. Increasing atomic species in HEAs elevates θ_D, thereby reducing T_c. For comparison samples, T_c increases when the e/a ratio rises from 4 to 5, but drops below 4.2 K when e/a exceeds 5. However, for multiphase or heterogeneous alloys, e/a alone cannot fully predict T_c.

4.2 Elemental substitution

Krnel et al[41] investigated the effects of Sc substitution on the structure, microstructure, and superconductivity of equiatomic HEAs. Nine Sc-containing HEAs were synthesized via arc melting, including ScHfNbTaTi, ScHfNbTaZr, and ScNbTaTiZr, which can be regarded as Sc-substituted derivatives of the Ta-Nb-Hf-Zr-Ti system. Most alloys exhibit dual-phase structures: one bcc phase and one Sc-rich hexagonal close-packed (hcp) phase. Notably, ScHfNbTaZr contains two bcc phases and one hcp phase. Superconducting properties (summarized in Table 1) reveal exceptional upper critical field performance in these three systems. Superconductivity originates exclusively from the bcc phase, whose parameters closely match those of the bcc phase in the Hf-Nb-Ta-Ti-Zr parent alloy, while the Sc-containing hcp phase remains non-superconducting.

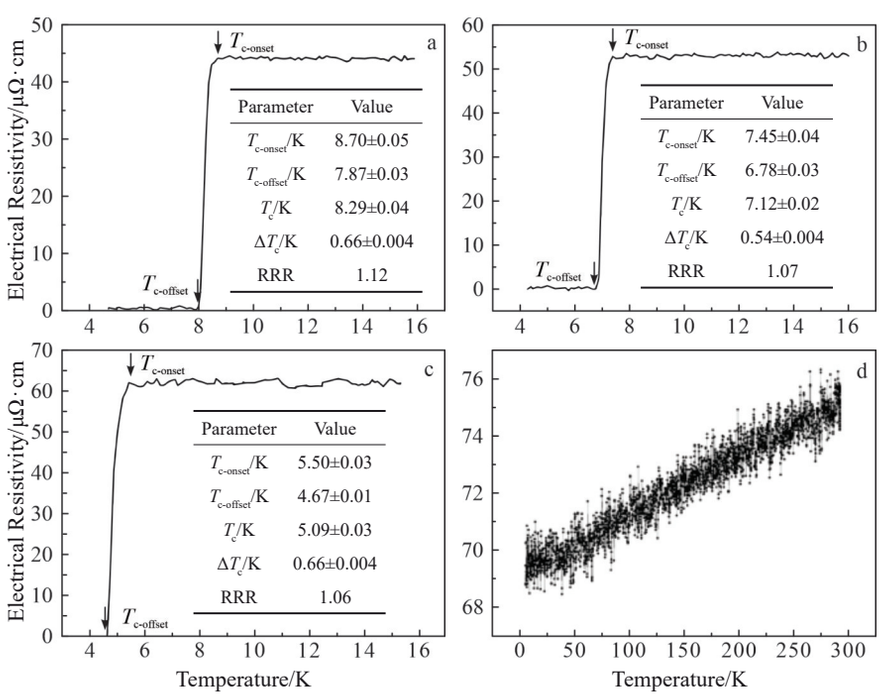

Fig.1 Electrical resistivity-temperature curves from 4.2 K to 300 K in the absence of a magnetic field for as-cast HEAs[35]: (a) C4, (b) C5, (c) C6, and (d) C7

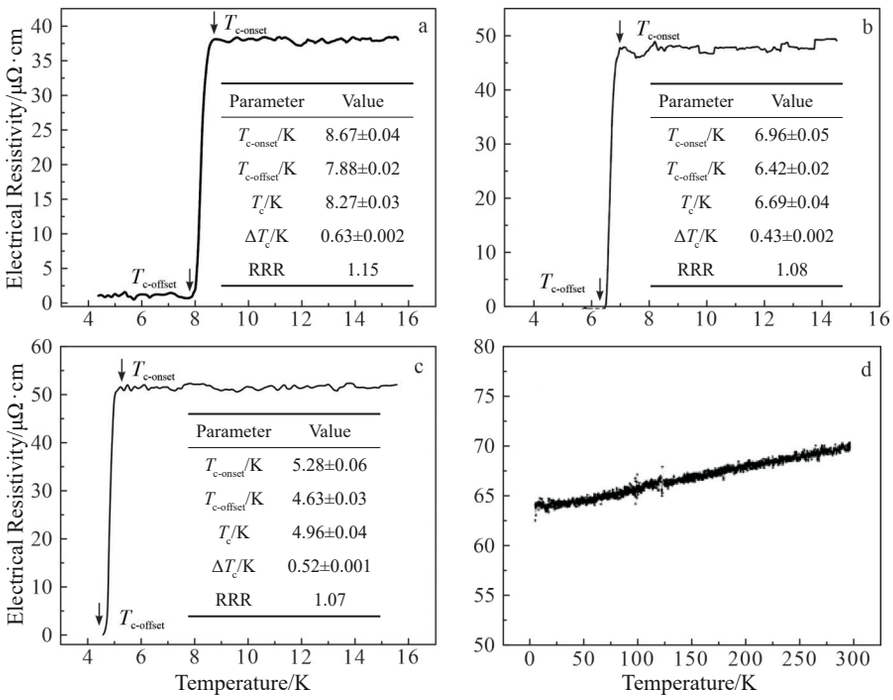

Fig.2 Electrical resistivity-temperature curves from 4.2 K to 300 K in the absence of a magnetic field for homogenized HEAs[35]: (a) H4, (b) H5, (c) H6, and (d) H7

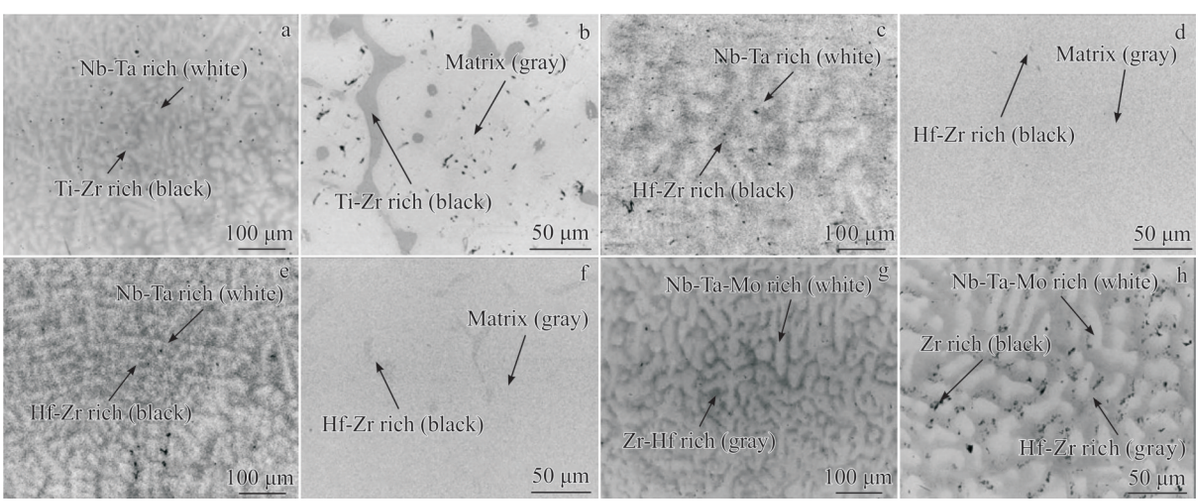

Fig.3 Back-scattered electron images for as-cast and homogenized HEAs[35]: (a) C4, (b) H4, (c) C5, (d) H5, (e) C6, (f) H6, (g) C7, and (h) H7

Von Rohr et al[39] studied the impact of isoelectronic substitution (VEC=4 or 5) in bcc-structured Ta-Nb-Zr-Hf-Ti superconductors by replacing elements with Mo-Y, Mo-Sc, and Cr-Sc mixtures via arc melting. Fig. 4 shows the magnetization curve of the doped sample, and Table 2 summarizes the corresponding T_c. The T_c of Sc-Cr doped sample (Fig.4a) is 5.6 K, while the T_c of Y-Mo doped (Fig.4b) and Sc-Mo doped (Fig. 4c) samples are reduced to 4.7 and 4.4 K, respectively, indicating that the substitution of element Nb has a significant impact on the superconductivity. Key findings include (1) Hf/Ti substitution: negligible variation in T_c; (2) Zr substitution: slight T_c reduction across three substitution cases, indicating critical role of Zr in achieving the original T_c≈7.6 K; (3) Nb substitution: dramatically suppressed T_c, confirming essential contribution of Nb to optimizing superconducting transitions in HEAs.

Nelson et al[38] creatively prepared $(TaNb)_{0.31}(TiUHf)_{0.69}$ by replacing Zr with U by arc melting method, which also has bcc structure and lattice constant of 0.341 nm. The lattice parameters of other Ta-Nb-Hf-Zr-Ti HEAs are generally less than 0.34 nm, and the material has strong corrosion resistance and is insoluble in 16 mol/L concentrated nitric acid, 9 mol/L hydrobromic acid, and aqua regia. Its initial transition temperature of T_c≈3.2 K and upper critical field of H_{c2}≈6.4 T are higher than those of most U-based superconductors, but behind the average level of the system. The introduction of

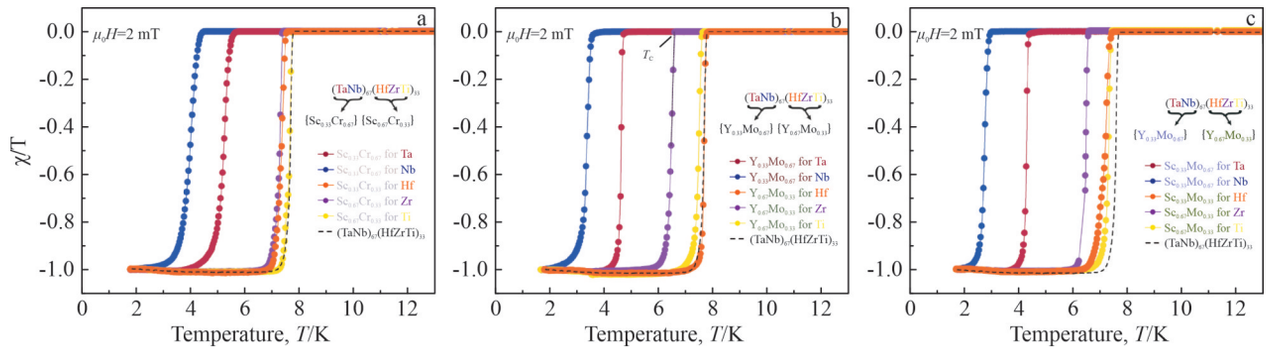

Fig.4 Temperature-dependent magnetization curves in units of 1/4π in a field of μ_0H=2 mT of the pristine HEA superconductor $(TaNb)_{0.67}(HfZrTi)_{0.33}$ substituted with isoelectronic Sc-Cr (a), Y-Mo (b), and Sc-Mo (c) mixtures[39]

Table 2 T_c for isoelectronic substitutions with Sc-Cr, Y-Mo, and Sc-Mo mixtures[39]

	Ta	Nb	Hf	Zr	Ti
$Sc_{0.33}Cr_{0.67}$	5.6	4.4	-	-	-
$Sc_{0.67}Cr_{0.33}$	-	-	7.5	7.4	7.6
$Y_{0.33}Mo_{0.67}$	4.7	3.5	-	-	-
$Y_{0.67}Mo_{0.33}$	-	-	7.6	6.7	7.5
$Sc_{0.33}Mo_{0.67}$	4.4	2.9	-	-	-
$Sc_{0.67}Mo_{0.33}$	-	-	7.5	6.6	7.5

uranium may weaken the superconductivity by enhancing the disorder. In addition, its superconductivity is not sensitive to pressure[7]. This shows that it is possible to use other radioactive elements to replace and create more HEAs, which lays a foundation for the study of the direct impact and long-term stability of natural radiation damage. In addition, the authors mentioned that Zr-containing analogues and HEAs have high strength, ductility, and damage resistance in a wide temperature range, which provides theoretical support for the radiation resistance of HEAs. Jung et al[33] prepared $TaNb_2HfZrTi$ thin film on Al_2O_3 substrate by PLD technique, which has significant resistance to displacement damage caused by irradiation, showing about 1000 times higher resistance to radiation damage than other superconducting materials. It means that Ta-Nb-Hf-Zr-Ti HEAs have the potential of anti-radiation application.

4.3 Lattice distortion

Wu et al[35] reported that increasing atomic species in Nb-Ta-Ti-Zr-based HEAs amplifies lattice distortion, thereby reducing T_c, indicating a detrimental effect of lattice distortion on superconductivity. Mota et al[42] investigated fcc-structured noble metal alloys with varying impurity contents, demonstrating that both compressive and expansive lattice distortions (induced by higher impurity concentrations) degrade T_c. Ramakrishnan et al[43] observed higher Debye temperatures in ternary $Nb_{50}Ti_{30}M_{20}$ (M=Mo, Pt, Pd, V, Ru) alloys compared to $Nb_{60}Ti_{40}$, correlating their lower T_c values with lattice distortion from increased elemental diversity.

The effect of lattice distortion on superconductivity is not absolute, and appropriate lattice distortion can increase EPC strength, thereby increasing T_c value and even obtaining excellent performance. Guo et al[36] studied the superconductivity of $(TaNb)_{0.67}(HfZrTi)_{0.33}$ HEAs under pressure of up to 190.6 GPa. They found that the T_c of the alloy was 7.7 K at normal pressure, which gradually increased to 10 K at 60 GPa, and then slowly decreased to 9 K at 190.6 GPa. XRD measurements at high pressures show that the alloy maintains a bcc structure at pressure up to 96 GPa and is compressed by about 28vol% . Further linear extrapolation shows that the volume is compressed by about 53vol% at 190 GPa. These results show that lattice distortion has a significant effect on superconductivity.

4.4 Electronic structure

Superconductivity strongly correlates with DOS near the Fermi level (E_F). Elevated DOS facilitates more electrons participating in Cooper pairing, enhancing T_c. In HEAs, multi-elemental randomness typically broadens DOS near E_F, favoring superconductivity. The electron phonon coupling parameter λ is the sum of the interactions between all conduction electrons and phonons on the Fermi surface in a polyatomic system. McMillan et al[44] studied the dependence of λ on various metal properties. For a given material category, the coupling constant is mainly determined by the phonon frequency, rather than the electronic properties. This finding shows that the sensitivity of transition temperature to lattice stiffness is higher than the electronic DOS, that is, T_c depends on the stiffness of the lattice related to λ, in which the softer lattice usually has larger λ and higher T_c. It is in good agreement with the numerical results in a wide range of parameters. The McMillan formula[44], derived from Eliashberg theory, is expressed as follows:

$$T_c = \frac{\theta_D}{1.45}\exp\left[-\frac{1.04(1+\lambda)}{\lambda-\mu^*(1+0.62\lambda)}\right] \quad (1)$$

where μ^* denotes the Coulomb pseudopotential. For most metals, $\mu^*\approx0.13$. The formula is derived based on the special assumption that the shape of the phonon DOS is equal to the shape of niobium. In this research, Debye is used as the characteristic phonon frequency, and the maximum phonon frequency ω_0 or the average phonon frequency $<\omega>$ can also be used. The model shows that the influence weight of λ on T_c is 1.5–2.0 times of θ_D, so lattice dynamics rather than

electronic DOS is the key factor to control T_c.

Wu et al[35] studied Fe/Ge/Hf-doped equimolar Nb-Ta-Ti-Zr HEAs, calculating $D(E_F)$ via susceptibility measurements. Results showed increased that DOS with elemental diversity but reduced T_c, confirming that DOS alone cannot dictate T_c. Matthias' empirical rule aligns with experiment results: T_c peaks at e/a=4.6–4.8.

4.5 Configurational entropy

Von Rohr et al[45] synthesized a series of $(TaNb)_{1-x}(ZrHfTi)_x$ superconductors by argon shielded arc melting using high purity metal sheets as raw materials to study the relationship between the mixing entropy of A-type HEAs and the critical temperature T_c. It is found that the increase in mixing entropy has no effect on T_c. The high disorder introduced by the increase in atomic species does not lead to the loss of superconductivity or the significant reduction in critical temperature T_c. However, the influence of element composition on the physical properties of highly disordered atoms on the simple lattice of superconducting HEA is significant. The linear relationship between the resistivity and temperature is typical for highly disordered alloys, which is caused by the short lifetime of the quasiparticles. These quasiparticles are dispersed disorderedly, resulting in decoherence, a phenomenon often referred to as inferior metal conductivity. The results show that the high configurational entropy of HEAs can stabilize the crystal structure. However, the increase in entropy of the A-type HEAs has an effect on the upper critical field, and the law is that the upper critical field increases with the increase in entropy.

4.6 Solid solution precipitation

Kim et al[34] studied the effect of thermal annealing on critical performance impact of arc-melted $Ta_{1/6}Nb_{2/6}Hf_{1/6}Zr_{1/6}Ti_{1/6}$. After the annealing temperature reaches 400 °C, the lattice parameters decrease rapidly and reach the minimum value at 700 °C. A similar phenomenon has been reported in equimolar HfNbTaTiZr[46–49]. Fig. 5 shows the relationships of T_c with thermal annealing temperature (T_a) and annealing time (t_a). Below 450 °C, T_c decreases with the increase in T_a, and then begins to increase, reaching a peak value at 800 °C. When T_a> 800 °C, it indicates that an inhomogeneous superconducting phase appears[50–51]. The dependence of T_c on t_a gradually increases with the prolongation of t_a. The $\mu_0 H_{c2}(0)$ value of the superconductor decreases monotonically with the increase in T_a and prolongation of t_a. After annealing at 1000 °C for 24 h and 550 °C for 48 h, the $\mu_0 H_{c2}(0)$ of the sample decreases from 13.27 T to 9.07 T and 10.95 T, respectively, which may be attributed to enhanced impurity scattering[52]. Similar to previously reported samples[15], it can be seen in Fig.6 that J_c (0) of the original sample is only 39 kA·cm^{-2} at 2 K and 28 kA·cm^{-2} at 4.2 K, and the J_c value drops rapidly in the magnetic field. The $J_c(0)$ at 4.2 K of the sample annealed at T_a= 550 °C for 24 h increases by about 1860% compared with that of the abovementioned sample, reaching approximately 520 kA·cm^{-2}. The magnetic field properties of samples after heat treatment are significantly improved, and the low-field J_c of HEAs can be further improved by inhibiting thermal instability.

In summary, the property regulation of HEAs is essentially a co-regulatory process of electron-phonon-lattice coupling in a multi-component disordered system. The low atom filling characteristic of bcc structure endows it with high critical field and anti-irradiation threshold by enhanced DOS and high-pressure stability, while the threshold effect of lattice distortion regulates phonon anharmonicity through local strain field, forming a micro-level equilibrium state: moderate disorder enhances EPC strength, while excessive distortion suppresses the Debye temperature. The non-substitutable and gap atom doping of element Nb/Zr reveal the decoupling design logic of structural support elements and functional regulatory elements, while the failure of traditional McMillan formula in a strongly disordered system and the DOS-T_c theory point to the central role of multi-phonon mode coupling and Fermi surface nesting effect in momentum space. It is urgent to develop a theory of non-equilibrium superconductivity including chemical disorder correction. The above experiments show that heat treatment can significantly improve the current carrying performance by regulating micro-defects, and the optimization process of such process parameters can be further accelerated by combining the prediction ability of machine learning.

5 Material Design of Ta-Nb-Hf-Zr-Ti HEAs

5.1 Design principles for HEAs

As described in Section 4.3, the lattice distortion caused by

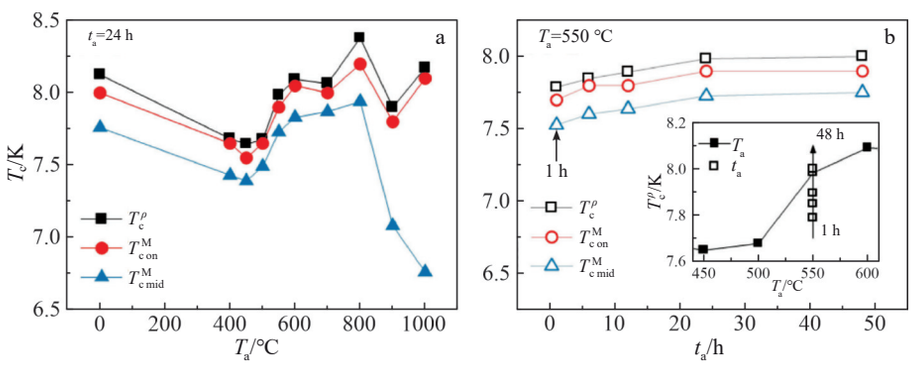

Fig.5 T_c of HEAs varying with annealing temperature (a) and annealing time (b)[34]

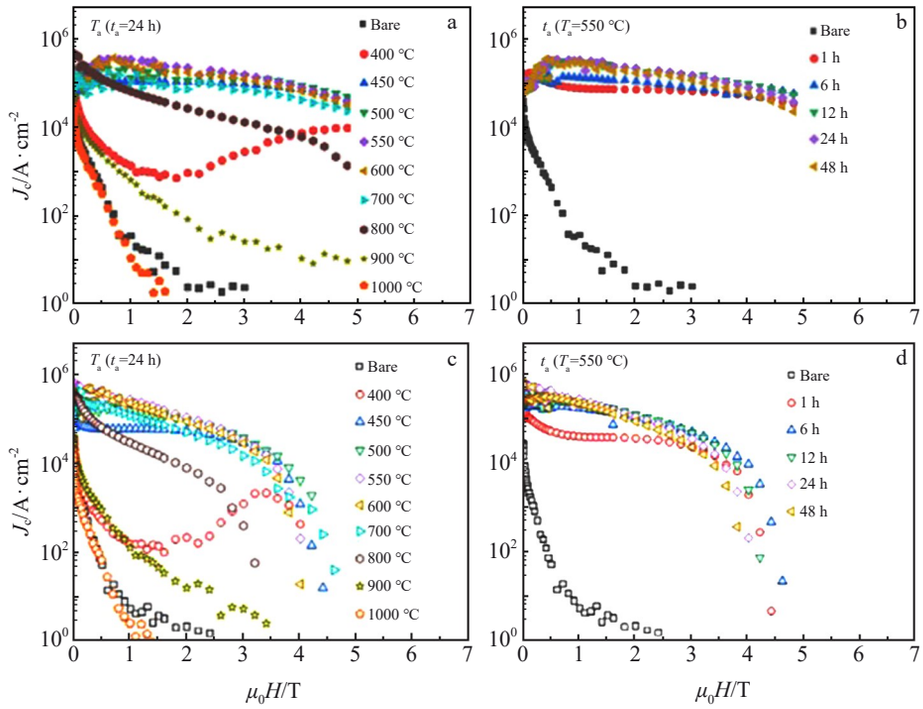

Fig.6 Magnetic field dependence of J_c at 2.0 K (a–b) and 4.2 K (c–d) for the HEAs with respect to T_a (a, c) and t_a (b, d)[34]

the increase in atomic species will inhibit T_c, so it is necessary to balance the entropy increase and structural stability in the composition design. In HEAs, the formation and stability of single-phase solid solution is the core issue in the field of HEA[53], which is not only related to the number, type, and distribution of constituent elements, but also closely related to Gibbs free energy of mixing. High mixing entropy reduces the free energy of the system and makes the material have a stable structure[3]. For an ideal solid solution, the mixing entropy per mole of the component system is given by Eq. (2).

$$\Delta S_{\text{mix}} = -R\sum_i c_i \ln c_i \tag{2}$$

where c_i represents the atomic percentage of component i. For equimolar alloys (c_i=1/n), Eq. (2) can be simplified to Eq.(3)[12]:

$$\Delta S_{\text{mix}} = R\ln n \tag{3}$$

The total entropy contains configurational, vibrational, magnetic dipole, and electronic disorder contributions, with configurational entropy dominating in HEAs. For practical calculations, non-configurational terms are often neglected. In non-ideal solutions, atomic interactions generate non-zero ΔH_{mix}.

$$\Delta H_{\text{mix}} = \sum_{i=1,\, j\neq 1}^{n} c_i c_j \Delta H_{\text{mix}}^{ij} \tag{4}$$

where $\Delta H_{\text{mix}}^{ij}$ accounts for atomic size mismatch-induced lattice distortions. Moderate ΔH_{mix} combined with dominant $T\Delta S_{\text{mix}}$ at elevated temperatures stabilizes solid solutions[45]. The parameters used to describe the difference in atomic size (δ) between components are given by Eq. (5):

$$\delta = 100\sqrt{\sum_{i-1}^{n} c_i\left(1-\frac{r_i}{\bar{r}}\right)} \tag{5}$$

where r_i is the atomic radius of element i and $\bar{r}$ is the average atomic radius. Electron concentration refers to the total number of electrons, including d-electrons, contained in the valence band[54–55]. This is commonly referred to as VEC[56]. VEC can be calculated as the weighted average of the VEC of each component, as shown in Eq.(6).

$$\text{VEC} = \sum_{i=1}^{n} c_i (\text{VEC})_i \tag{6}$$

where $(\text{VEC})_i$ is the valence electron count of element i. Fig. 7 illustrates the δ and VEC dependence of T_c in bcc-structured HEAs[9].

HEAs can be categorized into four types, where their crystal structures and T_c can be described by the VEC to determine the phase stability of intermetallic compounds[57–58], as shown in Table 3. VEC follows the empirical relationship of Matthias' rule[7,59–61], which links the maximum T_c to non-integer d-electron counts in simple binary alloys[61]. This rule suggests that T_c reaches its maximum at a VEC of

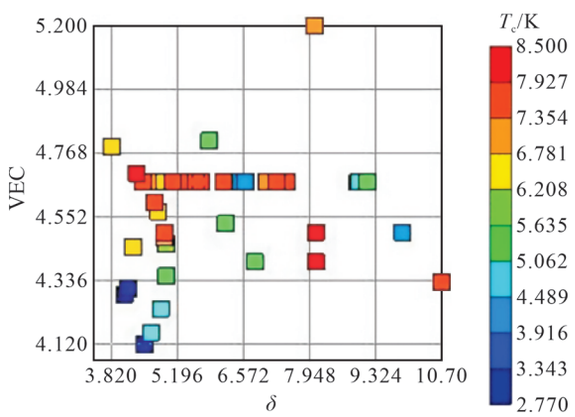

Fig.7 δ and VEC dependence of T_c for bcc-structured HEAs[9]

Table 3 Four types of HEAs[31]

Type	Crystal structure	T_c/K	VEC	Ref.
A	bcc	-	4.3–4.8	[7]
B	-	1.9–5.7	6.5–6.8	[62]
C	CsCl-type	3.9–9.3	5.9–6.3	[7]
D	hcp	4.4	5.8	[63]

approximately 4.6729. For example, HEAs with a VEC of approximately 4.3 – 4.8 exhibit a bcc structure, and their T_c gradually increases with the increase in VEC, peaking at approximately 8 K near VEC=4.7.

Zhang et al[4] synthesized $(TaNb)_{1-x}(ZrHfTi)_x$ thin films by magnetron sputtering under the condition of dynamic limited gas phase growth. Fig. 8 shows the superconducting transformation with different x values, and Fig. 9 shows the corresponding VEC values with different x values[35]. When x= 0.40, T_c reaches its maximum value of approximately 6.7 K, and the corresponding VEC is about 4.61, which is more consistent with the above mentioned, and the slight difference may be related to impurities, defects, and lattice distortion[35].

Currently, the design of HEAs remains constrained by the dual dilemmas of empirical rule dominance and unclear microscopic mechanisms. Although the VEC-δ diagram[9] offers a practical framework for component screening. The significant deviation between first-principles calculations and experimental values[28] indicates that the traditional Bardeen-Cooper-Schriffer theory exhibits fundamental restrictions in describing strongly disordered multi-component systems.

5.2 Computer-aided approaches in material design

In recent years, machine learning methods have been widely used in the design of HEA materials[64]. By building material databases, machine learning can predict the superconducting and mechanical properties of new materials. Zhou et al[65] used a variety of phase selection methods based on machine learning and introduced 13 parameters, including atomic size difference, mixing enthalpy, and electronegativity difference, among which artificial neural network showed the best accuracy. The sensitivity of each design parameter to different phase formation is analyzed by sensitivity matrix. The enthalpy of ideal mixing has a significant positive effect on the formation of solid solution, and the difference of atomic size has a strong negative effect.

For $Ta_{34}Nb_{33}Hf_8Zr_{14}Ti_{11}$ material, Jasiewicz et al[28] calculated its electronic structure and λ by the first principles. They used the Korringa-Kohn-Rostoker (KKR) method combined with the coherent potential approximation (CPA)[66] to solve the computational complexity caused by the complex electronic structure. Fig. 10 shows the total DOS (TDOS) and the contribution of each constituent atom. Fermi level (E_F) is at the peak of TDOS and partial DOS, as shown in Fig. 10b–10f, which is generally beneficial to superconductivity. Fig. 11 shows the image of the electron band. The black line represents the real part and the green line represents the imaginary part, which corresponds to the finite life cycle of

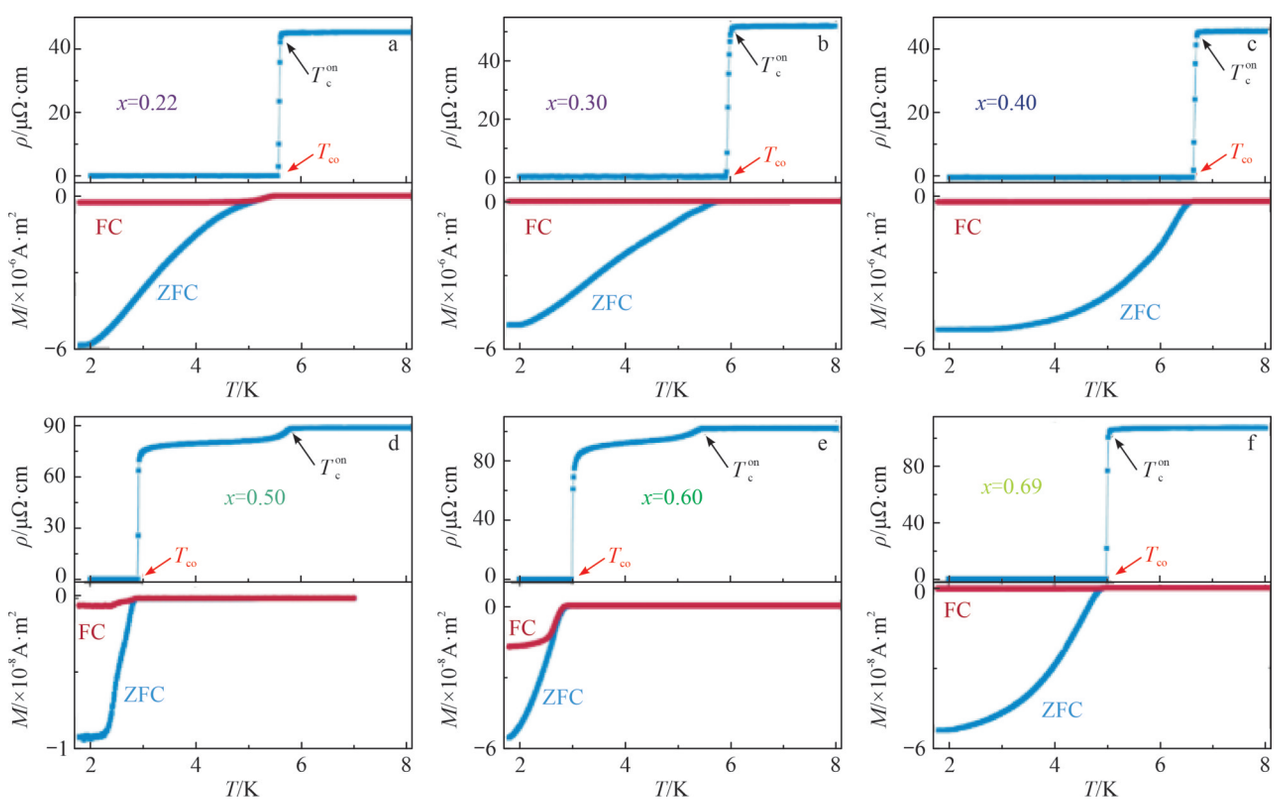

Fig.8 Normal-to-superconducting phase transitions of the $(TaNb)_{1-x}(ZrHfTi)_x$ films[4] (FC refers to field cooling curve, and ZFC means zero-field cooling curve): (a) x=0.22; (b) x=0.30; (c) x=0.40; (d) x=0.50; (e) x=0.60; (f) x=0.69

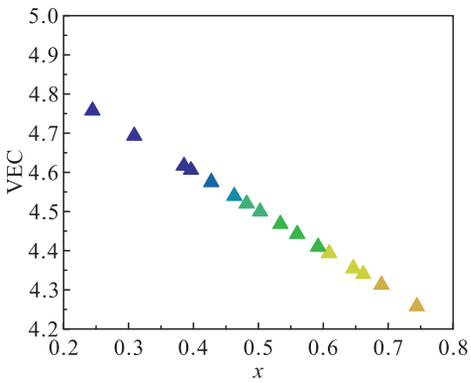

Fig.9 VEC values of $(TaNb)_{1-x}(ZrHfTi)_x$ thin films with different x values[35]

the electronic state. Although there is a great disorder among the five elements, the electron band is quite sharp. The calculated value of T_c is 15 K, while the experimental value is only 7.3 K. Such a huge difference may come from the rough estimation of the phonon part of EPC constant, and a large Coulomb pseudopotential μ^* (about 0.25) is required to make the theoretical calculation consistent with the experimental data. The λ=1.16±0.05 is close to the estimated λ=1 using the Sommerfeld coefficient, so $Ta_{34}Nb_{33}Hf_8Zr_{14}Ti_{11}$ alloy can be classified as a strong electron-phonon coupled superconductor.

Jasiewicz et al[67] examined the influence of pressure on the electronic structure and superconductivity of the $(TaNb)_{0.67}(HfZrTi)_{0.33}$ HEA, accurately predicting the T_c of HEAs using the first-principles calculations based on McMillan's formula. The electronic structure was computed using the KKR method combined with CPA. Subsequently, the rigid muffin tin approximation (RMTA) was employed to calculate the McMillan-Hopfield parameters based on the KKR-CPA results. Fig. 12 illustrates the TDOS and atomic densities under varying pressures. It is evident that the Fermi level coincides with the DOS peak, with the primary contribution to the TDOS originating from the *d*-orbitals of all constituent atoms. As pressure increases, enhanced hybridization and a significant reduction in cell volume lead to a decrease in DOS. Additionally, pressure increases the distance between the two highest DOS peaks and broadens the bandwidth. With the increase in pressure, TDOS at the Fermi level gradually decreases. At approximately 70 GPa, a Lifshitz transition is observed as one of the bands crossing the Fermi level. The calculated McMillan-Hopfield parameter increases

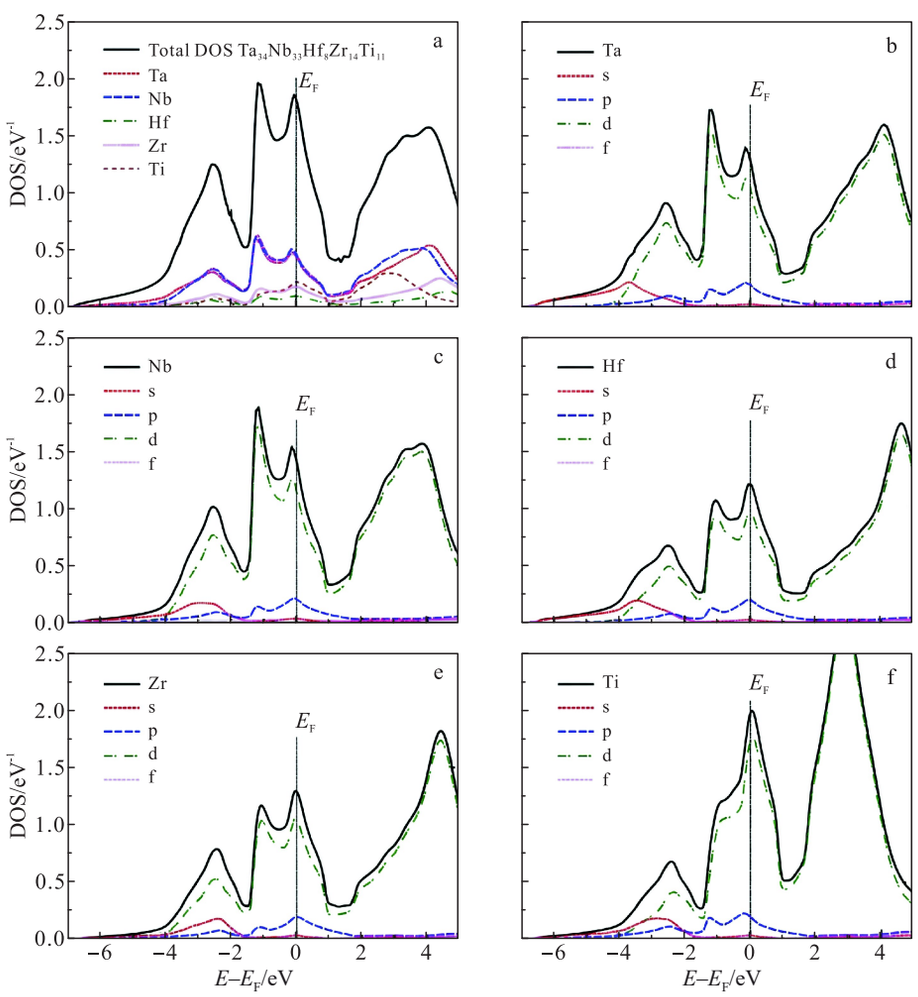

Fig.10 DOS of $Ta_{34}Nb_{33}Hf_8Zr_{14}Ti_{11}$[28]: (a) total DOS; (b–f) partial atomic densities with angular momentum decomposition

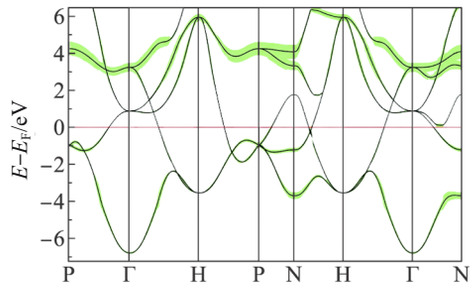

Fig.11 Electronic dispersion relations for $Ta_{34}Nb_{33}Hf_8Zr_{14}Ti_{11}$[28]

with the increase in pressure; however, λ decreases above 10 GPa due to lattice hardening and an increase in Debye temperature. These simulation results align well with experimental findings.

In summary, the design of HEAs has moved from empiricism to prediction based on multi-parameter calculations. Based on the thermodynamic framework of VEC threshold effect and Ω criterion, multi-parameter model driven by machine learning and first-principles calculation are used to realize cross-scale correlation of composition and structure. However, the current

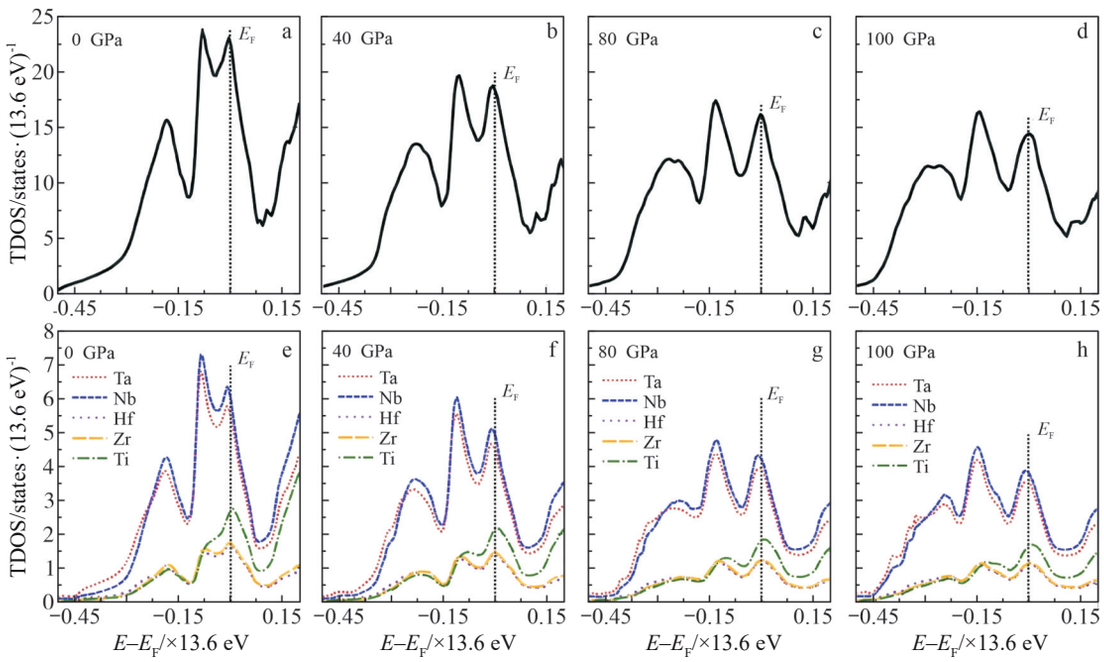

Fig.12 TDOS (a–d) and DOS (e–h) of Ta-Nb-Hf-Zr-Ti alloy calculated under various pressures[67]: (a, e) 0 GPa; (b, f) 40 GPa; (c, g) 80 GPa; (d, h) 100 GPa;

design is still restricted by the high price of rare elements and the inferior agreement between experimental result and theoretical prediction. The performance prediction combined with artificial intelligence may provide more accurate prediction results, and promote its leap from basic research to extreme scenarios, such as fusion reactor magnets and deep space detectors.

6 Conclusions and Perspectives

As a new generation superconducting material system, Ta-Nb-Hf-Zr-Ti HEA shows multiple advantages. (1) Critical parameter competitiveness: $H_{c2}(0)$ is up to 17.3 T, which is higher than that of commercial NbTi (H_{c2}≈11 T); (2) extreme environmental tolerance: the radiation damage threshold is >10 dpa, which is 100 times higher than that of traditional superconductors; (3) machinability breakthrough: the optimization of preparation process (such as SPS) makes the current carrying capacity of HEAs wire close to international thermonuclear experimental reactor standard, which shows the potential of engineering application. Future studies should explore its superconducting mechanism, optimize material design, and expand its application prospects in extreme environments. In particular, through machine learning and big data technologies, the process of discovery and optimization of new materials can be accelerated.

Although the superconductivity of Ta-Nb-Hf-Zr-Ti HEAs is close to NbTi at present, compared with Nb_3Sn and MgB_2 superconducting materials, it shows excellent properties in terms of mechanical strength, fracture resistance, wear resistance, corrosion resistance, oxidation resistance, high thermal stability, and structural stability. It is predicted that it will become one of the outstanding candidate materials for future superconducting magnet applications and applications under extreme conditions. Ta-Nb-Hf-Zr-Ti superconductors generally have a bcc crystal structure, their critical temperature is close to 10 K, and their critical field performance is excellent among HEAs and even the entire field of superconductors. The critical performance of HEAs is closely related to VEC, and the proportion of Nb and Zr should be paid attention to during the atomic ratio adjustment, which has a greater influence on T_c. However, in the case of system

determination, the variation range of VEC is relatively restricted, so the combination of pressure, doping, heat treatment, and other regulatory means to improve its performance may be a more effective way. Considering that the constituent elements of Ta-Nb-Hf-Zr-Ti and NbTi come from the same main family, the regulatory strategies of NbTi can be considered.

The early preparation of HEAs was mainly by arc melting. However, studies have shown that the superconductivity is extremely sensitive to the synthesis conditions. Among the HEAs prepared by SPS and arc melting methods, the samples prepared by SPS method show significant advantages in terms of critical parameters, which suggests that different preparation methods may lead to better performance. At present, a variety of superconductors of Ta-Nb-Hf-Zr-Ti system with different atomic ratios have been reported. Although the T_c values of materials with different composition do not change much, there are significant differences in $H_{c2}(0)$ values, which may mean that different atomic ratios focus on specific properties.

Based on current empirical knowledge, enhancing the superconducting performance of Ta-Nb-Hf-Zr-Ti HEAs requires a multifaceted approach. Firstly, optimizing preparation and post-processing techniques is critical to improving material homogeneity and intergranular connectivity, which directly enhances the J_c. Secondly, elemental doping and substitution must be carefully tailored. Studies suggest that moderate addition of elements like C and Fe can boost both the T_c and $H_{c2}(0)$, while elements such as Sc and Mo tend to degrade performance. Thirdly, the electronic structure design should be refined by leveraging the compositional flexibility of HEAs to adjust elemental ratios. This allows indirect tuning of VEC, a parameter deeply correlated with T_c, as predicted by Matthias ' rule. Finally, crystal structure regulation plays a pivotal role. Stabilizing the bcc phase through compositional adjustments can enhance H_{c2}, while applying controlled high pressure may strengthen EPC to elevate T_c, though excessive pressure risks suppressing superconductivity.

Although the research of HEAs is still in its infancy, the superconductivity of Ta-Nb-Hf-Zr-Ti system has been continuously optimized under the joint promotion of experimental and theoretical research, and remarkable achievements have been made. The superconducting current carrying capacity of the thin film sample at 4.2 K is as high as 10^3 kA·cm^{-2}, and the newly developed high-entropy wire can also reach 10^2 kA·cm^{-2}, which still exceeds the current practical superconducting material standards. What is particularly encouraging is that the anti-irradiation performance of the system has achieved a qualitative leap, reaching a hundred times higher than that of other practical superconductors, so it can show more excellent adaptability of magnetic confinement fusion superconducting magnets and hadron accelerator magnets in highly irradiated particle environment. With the continuous progress of preparation technique, the performance of HEAs will undoubtedly continue to improve and move to a new peak.

The research process of Ta-Nb-Hf-Zr-Ti HEAs perfectly explains the material design philosophy that unconventional properties come from unconventional structures. Its triple advantages, geometric rigidity (bcc frame) with anti-radiation performance, composition-affected critical parameters (VEC fine-tuning), and intrinsic stability under extreme conditions (high configurational entropy) make it irreplaceable in strategic fields, such as fusion reactor superconducting magnets and deep space detector power systems, and it is worth more efforts to explore and study. It is firmly believed that in the near future, with the continuous deepening of research and continuous progress of technology, HEAs will play their unique advantages in a wider range of fields and make important contributions to the sustainable development of human society.

References

1 Yeh J W, Chen S K, Lin S J *et al. Advanced Engineering Materials*[J], 2004, 6(5): 299

2 Cantor B, Chang I T H, Knight P *et al. Materials Science and Engineering A*[J], 2004, 375–377: 213

3 Youssef K M, Zaddach A J, Niu C N *et al. Materials Research Letters*[J], 2015, 3(2): 95

4 Zhang X F, Shu R, Liu H L *et al. Communications Physics*[J], 2022, 5(1): 7

5 Zhang X, Winter N, Witteveen C *et al. Physical Review Research*[J], 2020, 2(1): 013375

6 Kozelj P, Vrtnik S, Jelen A *et al. Physical Review Letters*[J], 2014, 113(10): 5

7 Sun L L, Cava R J. *Physical Review Materials*[J], 2019, 3(9): 10

8 Gao L, Ying T, Zhao Y *et al. Applied Physics Letters*[J], 2022, 120(9): 092602

9 Kitagawa J, Hamamoto S, Ishizu N. *Metals*[J], 2020, 10(8): 1078

10 Ye Y F, Wang Q, Lu J *et al. Materials Today*[J], 2016, 19(6): 349

11 Liu Guang, Chen Peng, Yao Xiyu *et al. Acta Metall Sin*[J], 2022, 58(8): 1055 (in Chinese)

12 Yeh J W. *JOM*[J], 2013, 65(12): 1759

13 Qin Gang. *Correlation Among Valence Electron Concentration and Microstructure and Properties for High Entropy Alloys*[D]. Harbin: Harbin Institute of Technology, 2020 (in Chinese)

14 Zeng L Y, Li L F, Li K *et al. NPG Asia Materials*[J], 2024, 16(1): 60

15 Kim G, Lee M H, Yun J H *et al. Acta Materialia*[J], 2020, 186: 250

16 Otto F, Yang Y, Bei H *et al. Acta Materialia*[J], 2013, 61(7): 2628

17 Kovalev I A, Kochanov G P, Rubtsov I D *et al. Russian Patent*, 2021103466[P]. 2021

18 Hruška P, Eijt S W H, Schut H *et al. Surface and Coatings*

Technology[J], 2025, 496: 131642

19 Zhang X, Eklund P, Shu R. *Applied Physics Letters*[J], 2023, 123(5): 051902

20 Nadzri N I M, Halin D S C, Abdullah M M A *et al. Coatings*[J], 2022, 12(12): 11

21 Kim J, Wakai A, Moridi A. *Journal of Materials Research*[J], 2020, 35(15): 1963

22 Li C, Liu Z Y, Fang X Y *et al. Procedia CIRP*[J], 2018, 71: 348

23 Chen S Y, Tong Y, Liaw P K. *Entropy*[J], 2018, 20(12): 937

24 Guo Yiqian, Guo Zhenghua, Li Zhiyong *et al. Rare Metal Materials and Engineering*[J], 2023, 52(8): 2965 (in Chinese)

25 Zhao Yanchun, Song Haizhuan, Ma Huwen *et al. Rare Metal Materials and Engineering*[J], 2024, 53(1): 102 (in Chinese)

26 Izadi M, Farzaneh A, Mohammed M *et al. Rapid Prototyping Journal*[J], 2020, 26(6): 1059

27 Guo S, Liu C T. *Progress in Natural Science: Materials International*[J], 2011, 21(6): 433

28 Jasiewicz K, Wiendlocha B, Korbeń P *et al. Physica Status Solidi-Rapid Research Letters*[J], 2016, 10(5): 415

29 Idczak R, Nowak W, Rusin B *et al. Materials*[J], 2023, 16(17): 16

30 Le T, Lee Y, Tran D T *et al. Journal of Alloys and Compounds*[J], 2024, 1008: 176863

31 Kim J H, Hidayati R, Jung S G *et al. Acta Materialia*[J], 2022, 232: 117971

32 Jung S G, Han Y, Kim J H *et al. Journal of Alloys and Compounds*[J], 2024, 995: 8

33 Jung S G, Han Y, Kim J H *et al. Nature Communications*[J], 2022, 13(1): 3373

34 Kim J, Jung S G, Han Y *et al. Journal of Materials Science & Technology*[J], 2024, 189: 60

35 Wu K Y, Chen S K, Wu J M. *Natural Science*[J], 2018, 10(3): 110

36 Guo J, Wang H, Von Rohr F *et al. Proceedings of the National Academy of Sciences*[J], 2017, 114(50): 13144

37 Sobota P, Rusin B, Gnida D *et al. Acta Materialia*[J], 2025, 285: 120666

38 Nelson W L, Chemey A T, Hertz M *et al. Sci Rep*[J], 2020, 10(1): 4717

39 Von Rohr F O, Cava R J. *Physical Review Materials*[J], 2018, 2(3): 7

40 Hidayati R, Kim J H, Kim G *et al. Current Applied Physics*[J], 2024, 59: 169

41 Krnel M, Jelen A, Vrtnik S *et al. Materials*[J], 2022, 15(3): 20

42 Mota A C, Hoyt R F. *Solid State Communications*[J], 1976, 20(10): 1025

43 Ramakrishnan S, Chandra G. *Solid State Communications*[J], 1985, 56(11): 965

44 McMillan W L. *Physical Review*[J], 1968, 167(2): 331

45 Von Rohr F, Winiarski M J, Tao J *et al. Proceedings of the National Academy of Sciences*[J], 2016, 113(46): E7144

46 Cao P P, Huang H L, Jiang S H *et al. Journal of Materials Science & Technology*[J], 2022, 122: 243

47 Senkov O N, Pilchak A L, Semiatin S L. *Metallurgical and Materials Transactions A*[J], 2018, 49A(7): 2876

48 Yasuda H Y, Yamada Y, Cho K *et al. Materials Science and Engineering A*[J], 2021, 809: 10

49 Chen S Y, Tong Y, Tseng K K *et al. Scripta Materialia*[J], 2019, 158: 50

50 Lv B, Deng L Z, Gooch M *et al. Proceedings of the National Academy of Sciences of the United States of America*[J], 2011, 108(38): 15705

51 Sun Y, Zhou W, Cui L J *et al. AIP Advances*[J], 2013, 3(10): 11

52 Chen G F, Chen Z G, Dong J *et al. Physical Review B*[J], 2009, 79(14): 140509

53 Wang S, Wu M, Shu D *et al. Acta Materialia*[J], 2020, 201: 517

54 Mizutani U. *Hume-Rothery Rule in Structurally Complex Alloy Phases*[C]. San Francisco: TMS, 2005: 1

55 Massalski T B. *Materials Transactions*[J], 2010, 51(4): 583

56 Guo S, Ng C, Lu J *et al. Journal of Applied Physics*[J], 2011, 109(10): 103505

57 Zhu J H, Liaw P K, Liu C T. *Materials Science and Engineering A*[J], 1997, 239: 260

58 Liu C T. *International Metals Reviews*[J], 1984, 29(1): 168

59 Liu B, Wu J F, Cui Y W *et al. Frontiers in Physics*[J], 2021, 9: 6

60 Marik S, Motla K, Varghese M *et al. Physical Review Materials*[J], 2019, 3(6): 6

61 Matthias B T. *Physical Review*[J], 1955, 97(1): 74

62 Stolze K, Tao J, Von Rohr F O *et al. Chemistry of Materials*[J], 2018, 30(3): 906

63 Marik S, Varghese M, Sajilesh K P *et al. Journal of Alloys and Compounds*[J], 2018, 769: 1059

64 Zhao Fengyuan, Ye Yicong, Zhang Zhouran *et al. Rare Metal Materials and Engineering*[J], 2023, 52(4): 1192 (in Chinese)

65 Zhou Z Q, Zhou Y J, He Q F *et al. npj Computational Materials* [J], 2019, 5: 128

66 Stopa T, Kaprzyk S, Tobola J. *Journal of Physics-Condensed Matter*[J], 2004, 16(28): 4921

67 Jasiewicz K, Wiendlocha B, Górnicka K *et al. Physical Review B*[J], 2019, 100(18): 184503

Ta-Nb-Hf-Zr-Ti高熵合金超导材料研究进展

曹立坤[1,2]，杨　芳[1]，郝清滨[2]，张胜楠[2]，闫　果[1,3]，张平祥[1,2]
(1. 西北工业大学 超导材料与应用技术研究院，陕西 西安 710072)
(2. 西北有色金属研究院 超导材料研究所，陕西 西安 710016)
(3. 西安聚能医工科技有限公司，陕西 西安 710028)

摘　要：高熵合金作为一类由多个主元素统计排列在简单晶格上构成的新型材料，因其出众的机械性能和独特的高熵特性，已成为材料科学和凝聚态物理领域的研究热点。自2014年第一个高熵超导体被发现以来，探索其在超导领域的性能与优势逐渐成为科研前沿。Ta-Nb-Hf-Zr-Ti体系高熵超导体在极端应用环境中展示了优秀的力学性能、卓越的抗辐射性能以及接近NbTi二元合金的超导性能，有望在高场超导磁体、超导电机和下一代核聚变反应堆等技术中应用。本文综述了Ta-Nb-Hf-Zr-Ti体系在超导体上的研究进展，旨在为该领域的发展提供参考。

关键词：高熵合金；Ta-Nb-Hf-Zr-Ti；超导材料

作者简介：曹立坤，男，2001年生，硕士生，西北工业大学超导材料与应用技术研究院，陕西 西安 710072，E-mail：caolikun@mail.nwpu.edu.cn